Subthalamic and pallidal stimulation in Parkinson's disease induce distinct brain topological reconstruction

Chunguang Chu [a,1], Naying He [b,1], Kristina Zeljic [c,1], Zhen Zhang [a], Jiang Wang [a], Jun Li [d], Yu Liu [b], Youmin Zhang [b], Bomin Sun [e,f], Dianyou Li [e,f], Fuhua Yan [b], Chencheng Zhang [e,f,g], Chen Liu [a,*]

[a] School of Electrical and Information Engineering, Tianjin University, Tianjin, China
[b] Department of Radiology, Ruijin Hospital, Shanghai Jiao Tong University School of Medicine, Shanghai, China
[c] School of Health Sciences, City, University of London, London, EC1V 0HB, UK
[d] School of Information Science and Technology, Shanghai Tech University, Shanghai, China
[e] Department of Neurosurgery, Center for Functional Neurosurgery, Ruijin Hospital, Shanghai Jiao Tong University School of Medicine, Shanghai, China
[f] Clinical Neuroscience Center, Ruijin Hospital LuWan Branch, Shanghai Jiao Tong University School of Medicine, Shanghai, China
[g] Shanghai Research Center for Brain Science and Brain-Inspired Technology, Shanghai, China

ARTICLE INFO

ABSTRACT

The subthalamic nucleus (STN) and globus pallidus internus (GPi) are the two most common and effective target brain areas for deep brain stimulation (DBS) treatment of advanced Parkinson's disease. Although DBS has been shown to restore functional neural circuits of this disorder, the changes in topological organization associated with active DBS of each target remain unknown. To investigate this, we acquired resting-state functional magnetic resonance imaging (fMRI) data from 34 medication-free patients with Parkinson's disease that had DBS electrodes implanted in either the subthalamic nucleus or internal globus pallidus ($n = 17$ each), in both ON and OFF DBS states. Sixteen age-matched healthy individuals were used as a control group. We evaluated the regional information processing capacity and transmission efficiency of brain networks with and without stimulation, and recorded how stimulation restructured the brain network topology of patients with Parkinson's disease. For both targets, the variation of local efficiency in motor brain regions was significantly correlated ($p < 0.05$) with improvement rate of the Uniform Parkinson's Disease Rating Scale-III scores, with comparable improvements in motor function for the two targets. However, non-motor brain regions showed changes in topological organization during active stimulation that were target-specific. Namely, targeting the STN decreased the information transmission of association, limbic and paralimbic regions, including the inferior frontal gyrus angle, insula, temporal pole, superior occipital gyri, and posterior cingulate, as evidenced by the simultaneous decrease of clustering coefficient and local efficiency. GPi-DBS had a similar effect on the caudate and lenticular nuclei, but enhanced information transmission in the cingulate gyrus. These effects were not present in the DBS-OFF state for GPi-DBS, but persisted for STN-DBS. Our results demonstrate that DBS to the STN and GPi induce distinct brain network topology reconstruction patterns, providing innovative theoretical evidence for deciphering the mechanism through which DBS affects disparate targets in the human brain.

1. Introduction

Parkinson's disease (PD) is a neurodegenerative disorder characterized by prominent motor symptoms together with cognitive and emotional disturbances. (Chaudhuri et al., 2006) Deep brain stimulation (DBS) is highly effective for the alleviation of motor complications in advanced PD, and has become a standard treatment option. (Deuschl et al., 2006) DBS involves placing an electrode in a target brain area of a pathological neural circuit and delivering electrical stimula-tion. (Boutet et al., 2021) The most common target sites for deep brain stimulation in PD are the internal globus pallidus (GPi) and the subthalamic nucleus (STN). Although the efficacy and safety of DBS in these targets for treating motor fluctuations and dyskinesia are well established (Lachenmayer et al., 2021; Bloem et al., 2021; Lozano et al., 2019; Limousin and Foltynie, 2019; Bove et al., 2021; Zhang et al., 2020), the mechanisms behind the therapeutic action of DBS are not fully understood. (Lozano et al., 2019; Picillo et al., 2016) A recent study suggested that a shared functional network may underlie motor symptom

alleviation in PD for both GPi and STN stimulation. (L. et al., 2021) However, changes in functional connectivity of other brain networks have been shown to be target-dependent. (Zhang et al., 2020; Zhang et al., 2021) Moreover, differences in brain-wide topological changes induced by GPi versus STN stimulation remain unknown.

Brain network abnormalities in patients with PD are not local or limited to several neural circuits but are large scale and distributed. It can be found that human brain networks are organized according to an highly efficient topology that combines large clustering coefficients (i.e., dense local cluster connections) with short average path lengths (i.e., critical long-distance connections), a so-called small-world characteristics. (Dubbelink et al., 2014; Bassett and Bullmore, 2006; Stam and van Straaten, 2012) The small-world attributes of the brain network reflect its functional needs to support information processing in local regions (modularization) and the network overall brain routing property (integration). (Watts and Strogatz, 1998; van den Heuvel and Sporns, 2019) Several studies have shown that PD induces abnormal topology of brain functional connectivity within multiple networks. (Skidmore et al., 2011; Baggio et al., 2014; Lebedev et al., 2014; Gorges et al., 2015; Luo et al., 2015; Putcha et al., 2015) Meanwhile, large-scale brain network analyses based on graph theory approaches have shown abnormal topological characteristics in PD. (Skidmore et al., 2011; Luo et al., 2015; Gottlich et al., 2013) Moreover, these changes in topological properties of brain networks reflect clinical manifestations of PD (Berman et al., 2016; Bullmore and Sporns, 2012; Latora and Marchiori, 2001). For example, Sule *et al.* (Tinaz et al., 2016) reported a significant positive correlation between the average whole-brain network LocE and total UPDRS-III scores, while Olde Dubbelink *et al.* (Dubbelink et al., 2014) observed that longitudinal variation in network topology was associated with deteriorative motor UPDRS-III scores and cognitive performance. Such findings support the clinical utility of topological measurements in PD diagnosis and disease progress monitoring.

A key remaining question is how topological abnormalities in PD are altered by DBS treatment. To address this, we take advantage of recent technological advancements that have made it possible to obtain functional magnetic resonance images of individuals with PD with their DBS systems switched on. We used complex network analysis techniques to calculate and compare regional and global topological features of the brain in the DBS ON and OFF states in 34 individuals with PD with DBS electrodes implanted in either the STN or GPi. Because loss of local efficiency and decentralization in motor regions are two known topological features of PD that emerge early on and worsen over time (Dubbelink et al., 2014), we hypothesized that we would find these topological changes in the off state, and that they may be reversed during active stimulation, regardless of target. Furthermore, because subthalamic stimulation is known to have a higher rate of neuropsychiatric effects, we anticipated topological changes in regions associated with depression and cognitive decline, such as posterior cingulate and angular gyrus in patients who received STN-DBS, but not in those with GPi-DBS.

2. Materials and methods

2.1. Participants and assessment

Thirty-four individuals with a diagnosis of Parkinson's disease in accordance with the Movement Disorder Society criteria, and aged between 40 and 76 years were included in this study. Patients were recruited from Shanghai Ruijin Hospital (Shanghai, China). From this sample, 17 patients (12 males and five females) had undergone DBS targeting the STN, and 17 patients (eight males and nine females) had undergone DBS targeting the GPi. The inclusion criteria were as follows: (a) right-handed patients with idiopathic PD treated with two quadripolar DBS electrodes (Medtronic 3387, Medtronic, USA; or SceneRay 1210, SceneRay, China); (b) at the state of medicine-off; (c) no metal implants

besides the DBS system; (d) no largely predominant non-motor symptoms of the disease with affective or cognitive impairment and no psychiatric comorbidities; (e) no excessive tremor that would invalidate the scan at rest. Sixteen age-matched (aged 49–71 years) healthy older adults (eight males and eight females) were recruited as a control group. None of the participants had contraindications to functional magnetic resonance imaging (fMRI).

2.2. Clinical evaluation

Disease severity was assessed following the motor part of the Movement Disorders Society (MDS) Uniform Parkinson's Disease Rating Scale-III (UPDRS-III). (Antonini et al., 2013) The evaluation process of patients in the on and off states of DBS was as follows: an experienced neurologist conducted a primary clinical evaluation by phone several days before the scanning. On the day of the fMRI scanning, motor functions in the DBS-ON and DBS-OFF states were assessed by a movement disorders specialist after overnight discontinuation of medication using the MDS UPDRS-III. The DBS-OFF state was addressed after an hour of rest and reappearance of the motor symptoms. The improvement was measured as the percentage change in the UPDRS-III scores between the DBS-ON and DBS-OFF states.

2.3. Image acquisition

T1 and resting state fMRI (rs-fMRI) images were acquired using a 1.5-T MRI machine (Aero, Siemens, Germany). After structural scanning, an rs-fMRI scan of ~8 min was performed for each patient. The scanning parameters were as follows: T1 imaging parameters: repetition time, 3400 ms; echo time, 3 ms; inversion time, 900 ms; flip angle, 8°; voxel size, $1.0 \times 1.0 \times 1.0$ mm; matrix, 224×216; and number of slices, 192. The rs-fMRI imaging parameters were as follows: 210 vol; repetition time, 2100 ms; echo time, 40 ms; flip angle, 90°; voxel size, $3.0 \times 3.0 \times 3.0$ mm; gap, 0.9 mm; matrix, 66×66; and number of slices, 37.

2.4. Resting-state functional mri data preprocessing

The rs-fMRI standard image data preprocessing was performed using the Data Processing and Analysis of Brain Imaging (DPABI) toolbox, Version 4.1 (http://rfmri.org/dpabi). (Yan et al., 2016) The main steps were as follows: (a) the first ten volumes of the rs-fMRI were removed to eliminate unstable data; (b) the images were realigned after slice timing correction to correct for head movement; (c) functional images were normalized to the Montreal Neurological Institute (MNI) space using the Diffeomorphic Anatomical Registration Through Exponentiated Lie Algebra (DARTEL) method. (Ashburner and Friston, 2011) Spatial smoothing was performed with a Gaussian kernel of $6 \times 6 \times 6$ mm full-width at half maximum. This removed the quadratic trend. White matter, cerebrospinal fluid signals, and Friston 24 head motion parameters were regressed out as nuisance covariates. (Friston et al., 1996) A bandpass filter was used to extract signals between 0.009 and 0.08 Hz.

2.5. Construction of intrinsic dynamic connectivity networks

The brain intrinsic connectivity networks are made up of nodes (respective brain regions) and edges (the functional connectivity between the nodes). (Bassett and neuroscience, 2017; Jin et al., 2021) The GRETNA 2.0.0 toolbox (https://www.nitrc.org/projects/gretna/) was used to perform brain network analysis. (Tommasin et al., 2020; Wang et al., 2015) The brain regions were segmented using a previously validated automatic anatomical labeling (AAL)-based template. (Tzourio-Mazoyer et al., 2002) The labeled template image divides the brain into 116 cerebral anatomical regions of interest (ROIs), 45 cortical and subcortical ROIs in each hemisphere and 26 cerebellum structure ROIs as shown in Supplementary Table 1. The rs-fMRI time series for

each ROI was obtained by averaging the voxel time series within it. Each ROI represented a brain intrinsic connectivity network node. The mean time series of each region was calculated by averaging the fMRI time series over all voxels within it. These anatomical ROIs were extracted using the MarsBaR toolbox (http://marsbar.sourceforge.net).

The dynamic connection process was estimated from these 116 time series of each subject by the widely used sliding window approach. (Erhardt et al., 2011) We determined the correlations between all the time series from pairs of brain regions using Pearson's correlation coefficients, resulting in a 116×116 connection matrix for each sliding window in each subject. To correct the non-normality of the correlation coefficients, a Fisher's r-to-z transformation algorithm was applied to calculate the z-score. (Liu et al., 2017) Each correlation matrix of each subject was then transformed into a binarization matrix with a specific sparsity S pattern. Sparsity S was defined as the ratio of the total number of edges in a network to the maximum possible number of edges. When the Pearson's correlation coefficients were greater than the sparsity S value, corresponding edges were assumed to exist in the brain network. (Jin et al., 2021; Lu et al., 2017) Setting a specific threshold for sparsity S ensured that the brain networks of all groups had the same wiring cost and guaranteed minimization of the effect of possible differences in global correlation strength between pairs of groups, thus enabling us to explore inter-group differences in relative network organization. (He et al., 2009) We set the threshold at a step size of 0.01 according to the sparsity S values (0.10~0.45) and repeatedly applied a threshold to each of the relevant matrices to investigate whether prominent small-world characteristics were present in the brain network of patients when the DBS was switched on and off in each of the stimulation targets (STN and GPi).

2.6. Dynamic topological metrics—regional and global network properties

The topology organization variability of the functional connectivity network (FCN) was examined using the graph theory approach based on the obtained 90×90 binarization matrices of the subjects. The brain function organizational characteristics were summarized as separation and integration components. (Watts and Strogatz, 1998; Collantoni et al., 2019) We separately calculated global parameters for the FCN regional and global dynamics of each subject including (a) small-world parameters involving the normalized clustering coefficient γ, normalized characteristic path length λ, and small-worldness σ. When $\gamma > 1$, $\lambda \approx 1$, and $\sigma > 1$, the network had a small-world property, expressing the optimal balance between the separation and integration of brain networks; (b) FCN parameters that involve the clustering coefficient (CC) and local efficiency (LocE). CC measures the extent to which one node in the network can be combined with other nodes into a tightly connected cluster that represents the local information processing capability of the network; LocE measures the level of information transmission between neighboring nodes, reflecting the ability of the network resist random attacks. (Claeys et al., 2013) The higher the CC of the brain region, the stronger the information processing ability of the brain region, and the higher the LocE, the higher the information transmission efficiency between the brain region and other brain regions. The specific calculation formulas for the various parameters are presented in the Supplementary Text.

2.7. Statistical analysis

The two-sample t-test was performed to detect differences in age and the Chi-square test was performed to demonstrate differences in sex. Statistical significance level was set at $p < 0.05$. A series of two-sample t-tests ($p < 0.05$, with false discovery rate [FDR] correction) compared pairs of groups to detect significant differences in CC and LocE of regional FCN. This analysis included the healthy controls (HC) and patients with PD with the DBS at the ON or OFF state for the STN and GPi, separately. Statistical analyses were then carried out with MATLAB

(MathWorks Inc., Natick, MA, USA) using the SPM 12 software program (Wellcome Department of Cognitive Neurology, London, UK). The Brain-Net Viewer (https://www.nitrc.org/projects/bnv) was used to visualize the results, and the statistical maps were analyzed using the xjView software, which enabled us to identify significantly different brain regions. The Wilcoxon rank-sum test tested for significant differences in global network properties between the groups as mentioned above ($p < 0.05$, with FDR correction). Spearman's correlations quantified the linear relationship between the clinical UPDRS-III scores and global brain network topology parameters in patients with Parkinson's disease. The FDR correction adjusted the p-values for multiple comparisons, and the significance level was set to $p < 0.05$.

3. Results

3.1. Demographic and clinical characteristics

The patient and healthy control groups did not differ in sex ratio, age and improvement rate of UPDRS-III scores. Furthermore, disease durations and bilateral electrode DBS pulse widths were similar in the STN and GPi groups (all $p > 0.05$). Duration since DBS implantation, bilateral DBS electrode frequency and voltage were significantly higher in the GPi group than in the STN group (all $p < 0.05$). Detailed participant demographics and DBS parameters are shown in Table 1. Changes in topological features of the brain network were not significantly associated with sex, duration since DBS implantation, bilateral DBS electrode frequency or voltage (see Supplementary Table 2 and Table 3).

3.2. Small-world properties of the intrinsic brain network

By building intrinsic brain functional networks, we found that the network topology structure parameters in the sparsity threshold range of 0.01–0.45 in all participants (DBS ON or OFF for the patients) met the $\gamma > 1$, $\lambda \approx 1$, and $\sigma > 1$ conditions. This indicated that these networks exhibited typical characteristics of small-worldness, consistent with previous reports. (Schadt et al., 2006; Claeys et al., 2013) The detailed results are shown in Supplementary Fig. 1.

3.3. Identification of regional network topology

During the analysis of features in regional network topology, we found that STN-DBS and GPI-DBS induced topological changes in many different brain regions. We divided these regions with significant intergroup differences in CC and LocE into motor and non-motor brain regions for respective analysis. Next, we analyzed the CC and LocE of characteristic motor-related brain regions (precentral gyrus and supplementary motor area, as shown in Fig. 1A). We analyzed differences in characteristic motor brain region network attributes for all patients in the DBS-ON and DBS-OFF states; results are shown in Table 2. The average CC and LocE of the motor brain region network (regardless of target) in PD patients when DBS was switched on were significantly higher than those when DBS was switched off, and were closer to values of HC's. This indicates that DBS significantly improved CC and LocE in motor brain regions (precentral gyrus and supplementary motor area) for both STN or GPi. Furthermore, we found comparable alterations ($p > 0.05$) in topological parameters induced by STN-DBS and GPi-DBS (the alterations in topology parameters in the motor cortices induced by STN-DBS and GPi-DBS were similar (CC: $t = -0.026$, $p = 0.980$; LocE: $t = -0.316$, $p = 0.756$) as shown in Table 3. DBS to both STN and GPi targets exhibited significant effects on the motor functional network topology parameters, consistent with DBS-induced increase in brain interval information processing efficiency and the transmission efficiency of mean parallel information in the functional brain network of patients with Parkinson's disease.

We then investigated the correlation between the effect of DBS (STN/GPi) on motor functional brain regions and the improvement rate

Table 1
Participant demographic, clinical characteristics, and DBS parameters.

Characteristic	Patients with STN-DBS	Patients with GPi-DBS	Healthy controls	Group comparisons STN vs. HC	GPi vs. HC	STN vs. GPi
Sex	13 M, 4 F	7 M, 10 F	8 M, 8 F	X (*Deuschl et al., 2006*) = 2.496 p = 0.114	X (*Deuschl et al., 2006*) = 0.259 p = 0.611	X (*Deuschl et al., 2006*) = 4.371 *p = 0.037
Age (year)	62.7 (*7.9*)	62.1 (*8.9*)	60.3 (*7.4*)	t = 0.921 p = 0.364	t = 0.651 p = 0.520	t = 0.204 p = 0.840
Disease duration (year)	9.7 (*4.5*)	9.0 (*2.7*)	–	–	–	t = 0.625 p = 0.541
Duration since DBS implantation (month)	8.4 (*4.3*)	15.9 (*8.5*)	–	–	–	t = 3.090 *p = 0.007
DBS pulse width–left-side electrode (μs)	65.9 (*10.0*)	68.8 (*11.7*)	–	–	–	t = 0.788 p = 0.436
DBS frequency–left-side electrode (Hz)	117.1 (*25.1*)	142.6 (*14.8*)	–	–	–	t = 3.624 *p < 0.001
DBS voltage–left-side electrode (volts)	2.7 (*0.5*)	3.3 (*0.6*)	–	–	–	t = 3.071 *p = 0.004
DBS pulse width–right-side electrode (μs)	66.5 (*10.0*)	65.3 (*9.4*)	–	–	–	t = 0.354 p = 0.726
DBS frequency–right-side electrode (Hz)	117.1 (*25.1*)	142.6 (*14.8*)	–	–	–	t = 3.624 *p < 0.001
DBS voltage–right-side electrode (volts)	2.6 (*0.4*)	3.1 (*0.5*)	–	–	–	t = 3.482 *p = 0.002
Improvement rate of UPDRS-III scores	35.9 (19.3)	24.7 (15.8)	–	–	–	t = 2.057 p = 0.056

Values in the table are presented as mean (*S.D.*). The *p*-values were calculated using Chi-squared test for sex and two-sample *t*-test for all other variables included in the table. Significant differences ($p < 0.05$) are marked with an asterisk (*p). DBS = deep brain stimulation; F = female; GPi = globus pallidus internus; HC = healthy controls; *M* = male; SD = standard deviation; STN = subthalamic nucleus.
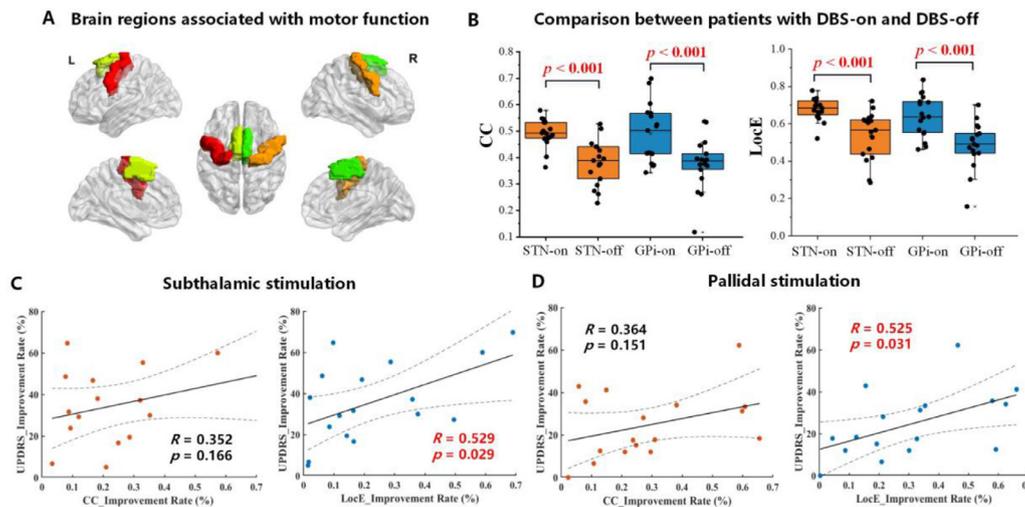

Fig. 1. Correlation of UPDRS-III motor symptom score improvement degree with motor functional network topology parameters in Parkinson's disease sample. (A) Brain regions associated with motor function. (B) Comparison of CC and LocE of characteristic motor networks between patients with DBS-on and DBS-off. (C) Deep brain stimulation (DBS) of the subthalamic nucleus (STN). (D) DBS of the globus pallidus internus (GPi). False discovery rate (FDR) corrected correlations significant at $p < 0.05$ are marked in red. CC = clustering coefficient; LocE = local efficiency; UPDRS-III = section three of the Uniform Parkinson's Disease Rating Scale.

Table 2
The alterations in topology parameters in the motor regions induced by STN-DBS and GPi-DBS.

Topology parameters	Patients with DBS-ON	Healthy controls	Patients with DBS-OFF	Group comparisons ON vs. HC	HC vs. OFF	ON vs. OFF
CC (STN-DBS)	0.49 (*0.05*)	0.49 (*0.12*)	0.38 (*0.08*)	t = 0.161 p = 0.874	t = 2.858 *p = 0.012	t = 5.453 *p < 0.001
LocE (STN-DBS)	0.68 (*0.06*)	0.63 (*0.14*)	0.54 (*0.13*)	t = 1.369 p = 0.191	t = 1.839 p = 0.086	t = 4.374 *p < 0.001
CC (GPi-DBS)	0.49 (*0.11*)	0.49 (*0.12*)	0.38 (*0.10*)	t = −0.315 p = 0.757	t = 4.249 *p = 0.001	t = 6.649 *p < 0.001
LocE (GPi -DBS)	0.64 (*0.06*)	0.63 (*0.11*)	0.49 (*0.13*)	t = 0.005 p = 0.996	t = 4.555 *p < 0.001	t = 6.970 *p < 0.001

Values in the table are presented as mean (S.D.). The p-values were calculated using two-sample *t*-test for variables included in the table. Significant differences ($p < 0.05$) are marked with an asterisk (*p). DBS = deep brain stimulation; GPi = globus pallidus internus; HC = healthy controls; S.D. = standard deviation; STN = subthalamic nucleus.

Table 3

The alterations in topology parameters in the motor cortices induced by STN-DBS and GPi-DBS.

Topology parameters	Parameter variation induced by DBS		The two-sample *t*-test	
	STN-DBS	GPi-DBS	*t* value	*p* value
CC	0.114 (*0.087*)	0.115 (*0.071*)	−0.026	0.980
LocE	0.143 (*0.135*)	0.156 (*0.092*)	−0.316	0.756

Values in the table are presented as mean (*S.D.*). DBS = deep brain stimulation; GPi = globus pallidus internus; STN = subthalamic nucleus; CC = clustering coefficient; LocE= local efficiency.
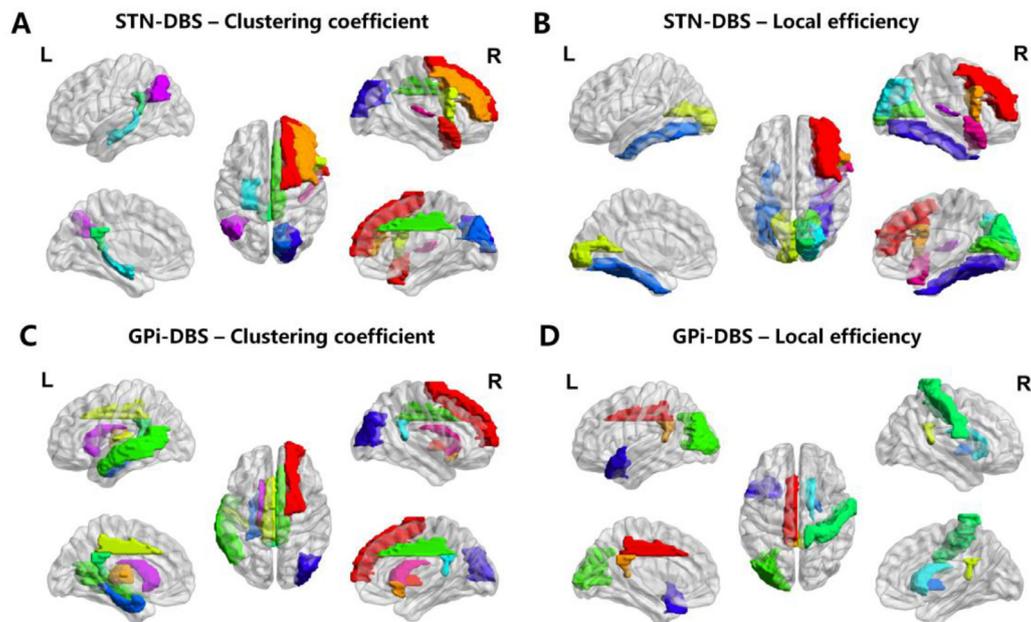

Fig. 2. Non-motor brain regions with significant changes in local network parameters. (A) STN-DBS - Clustering coefficient. (B) STN-DBS - Local efficiency. (C) GPi-DBS - Clustering coefficient. (D) GPi-DBS - Local efficiency. GPi-DBS = Parkinson's disease patients with deep brain stimulation (DBS) to the globus pallidus internus (GPi); *L* = left; *R* = right; STN-DBS = Parkinson's disease patients with DBS to the subthalamic nucleus (STN).

of UPDRS-III scores (see Fig. 1C and 1D). Importantly, we found under the influence of DBS, regardless of target (STN and GPi), there was a significant positive correlation between the changes in LocE of brain regions responsible for motor function and the UPDRS-III scores (STN, $R = 0.529$; GPi, $R = 0.525$; $p < 0.05$; FDR corrected).

We further found the locations of non-motor brain regions with significant differences in CC and LocE affected by the two DBS targets, as shown in Fig. 2 and Fig. 3. When STN was targeted (Fig. 3A right map), we found that the CC in the right median cingulate and paracingulate gyri (DCG.R) and left angular gyrus (ANG.L) was higher in the DBS-ON state than in the DBS-OFF state, while it was lower in the DBS-ON state than in the DBS-OFF state in the right superior frontal gyrus-dorsolateral (SFGdor.R), right middle frontal gyrus (MFG.R), right inferior frontal gyrus-opercular part (IFGoperc.R), left posterior cingulate gyrus (PCG.L), left hippocampus (HIP.L), right cuneus (CUN.R), right superior occipital gyrus (SOG.R), right Heschl's gyrus (HES.R), and right temporal pole: superior temporal gyrus (TPOsup.R). The regional LocE of the network was lower in the DBS-ON state than in the DBS-OFF state in the MFG.R, IFGoperc.R, right calcarine fissure and surrounding cortex (CAL.R), CUN.R, SOG.R, right fusiform gyrus (FFG.R), HES.R, TPOsup.R, left fusiform gyrus (FFG.L), and left calcarine fissure and surrounding cortex (CAL.L). For above brain regions, the variation in parameters was consistent across individuals. These satisfied the individual characteristics of the group. These brain regions are involved in the association, limbic and paralimbic networks. The association, limbic and paralimbic networks in all patients treated by STN-DBS showed decreased CC and LocE under the action of DBS-ON (Fig. 3A, left map).

For the GPi group (Fig. 3B right map), the CC in the left thalamus (THA.L), left caudate nucleus (CAU.L), right caudate nucleus (CAU.R), and right lenticular nucleus-pallidum (PAL.R) in patients was lower with DBS-ON than in the DBS-OFF state, while it was higher with DBS in the SFGdor.R, the right olfactory cortex (OLF.R), left median cingulate and paracingulate gyri (DCG.L), DCG.R, PCG.L, right posterior cingulate gyrus (PCG.R), left parahippocampal gyrus (PHG.L), right middle occipital gyrus (MOG.R), and left Heschl's gyrus (HES.L). The regional LocE of the network with DBS-ON was lower than in the DBS-OFF state in the PAL.R and CAU.R, and higher in PCG.L, PCG.R, DCG.L, left middle occipital gyrus (MOG.L), left temporal pole: superior temporal gyrus (TPOsup.L), and right postcentral gyrus (PoCG.R). The effects of DBS when targeting the GPi were consistent with individual characteristics, and the global regions formed by the above brain components showed increased CC and LocE under the DBS-ON state (Fig. 3B left map), opposite to the effects of STN-DBS.

We further analyzed differences in characteristic brain region network attributes for all patients in the DBS-ON and DBS-OFF states and results are shown in Table 4. As shown in Fig. 4A, the average CC and LocE of the brain network when STN was targeted and DBS was switched on or off were significantly lower than in HC and lower when DBS was switched on than off (CC: ON vs. HC, $t = −4.006$, $p < 0.001$; HC vs. OFF, $t = 2.125$, $p = 0.039$; ON vs. OFF, $t = −2.878$, $p = 0.023$; LocE: ON vs. HC, $t = −3.586$, $p < 0.001$; HC vs. OFF, $t = 2.385$, $p = 0.037$; ON vs. OFF, $t = −2.310$, $p = 0.038$; FDR corrected). These results indicate that STN-DBS could significantly reduce the information transmission ability of the altered brain regions in patients with Parkinson's disease (Fig. 2A left), and this reduction effect persisted after DBS was turned
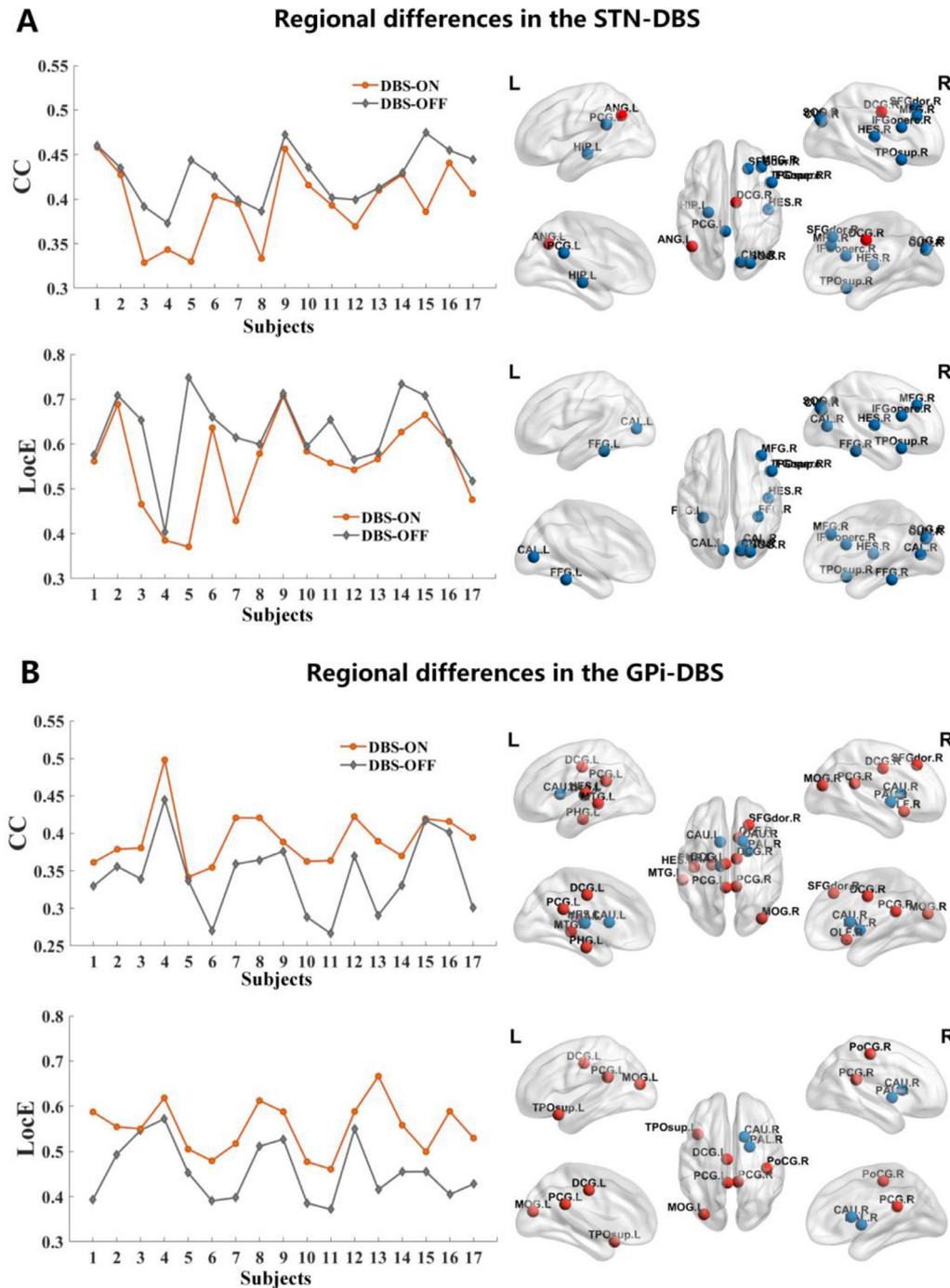
Fig. 3. Regional differences between Parkinson's disease patients in the DBS-ON and DBS-OFF states. (A) Regional differences in the STN-DBS. (B) Regional differences in the GPi-DBS. Individual differences are presented in the line charts. The marked dots on the brain maps represent the brain region locations that changed significantly in the DBS-ON state ($p < 0.05$, FDR corrected). The red dots represent a significant increase of the characteristic parameters in the DBS-ON state, while the blue dots represent a significant decrease. CC = clustering coefficient; DBS-OFF = patients with Parkinson's disease with the deep brain stimulation (DBS) switched off; DBS-ON = patients with Parkinson's disease with the DBS switched on; FDR = false discovery rate; L = left; LocE = local efficiency; GPi = globus pallidus internus; R = right; STN = subthalamic nucleus.

off. In contrast, when DBS was applied to the GPi group (Fig. 2B left and Fig. 4B), the average CC and LocE values were higher than in HC and in the DBS-OFF state (CC: ON vs. HC, $t = 6.298$, $p < 0.001$; ON vs. OFF, $t = 3.340$, $p = 0.003$; LocE: ON vs. HC, $t = 4.167$, $p < 0.001$; ON vs. OFF, $t = 6.270$, $p < 0.001$; FDR corrected). The average CC and LocE values of the DBS-OFF state in the GPi group and HC were similar (HC vs. OFF: CC, $t = -0.602$, $p = 0.597$; LocE, $t = -0.365$, $p = 0.721$; FDR corrected).

3.4. The reconstruction of dynamic network topology among individuals

In order to explore the dynamic influence of subthalamic and pallidal stimulation on brain network topology, we compared the overall brain dynamic network topology characteristics between patients in the DBS on and off states and healthy control subjects. Fig. 5 shows the distribution characteristics of the dynamic network parameters before and after applying the DBS in each patient. Specifically, the dynamic

Table 4

Comparison of topology parameters of the characteristic non-motor network.

Topology parameters	Patients with DBS-ON	Healthy controls	Patients with DBS-OFF	Group comparisons ON vs. HC	HC vs. OFF	ON vs. OFF
CC (STN-DBS)	0.40 (0.04)	0.45 (0.04)	0.43 (0.03)	$t = -4.006$ $*p < 0.001$	$t = 2.125$ $*p = 0.039$	$t = -2.878$ $*p = 0.023$
LocE (STN-DBS)	0.56 (0.10)	0.69 (0.07)	0.63 (0.09)	$t = -3.586$ $*p < 0.001$	$t = 2.385$ $*p = 0.037$	$t = -2.310$ $*p = 0.038$
CC (GPi-DBS)	0.39 (0.04)	0.33 (0.05)	0.34 (0.05)	$t = 6.298$ $*p < 0.001$	$t = -0.602$ $p = 0.597$	$t = 3.340$ $*p = 0.003$
LocE (GPi -DBS)	0.55 (0.06)	0.45 (0.07)	0.46 (0.07)	$t = 4.167$ $*p < 0.001$	$t = -0.365$ $p = 0.721$	$t = 6.270$ $*p < 0.001$

Values in the table are presented as mean (*S.D.*). The *p*-values were calculated using two-sample *t*-test for variables included in the table. Significant differences ($p < 0.05$) are marked with an asterisk (*p). DBS = deep brain stimulation; GPi = globus pallidus internus; HC = healthy controls; S.D. = standard deviation; STN = subthalamic nucleus.
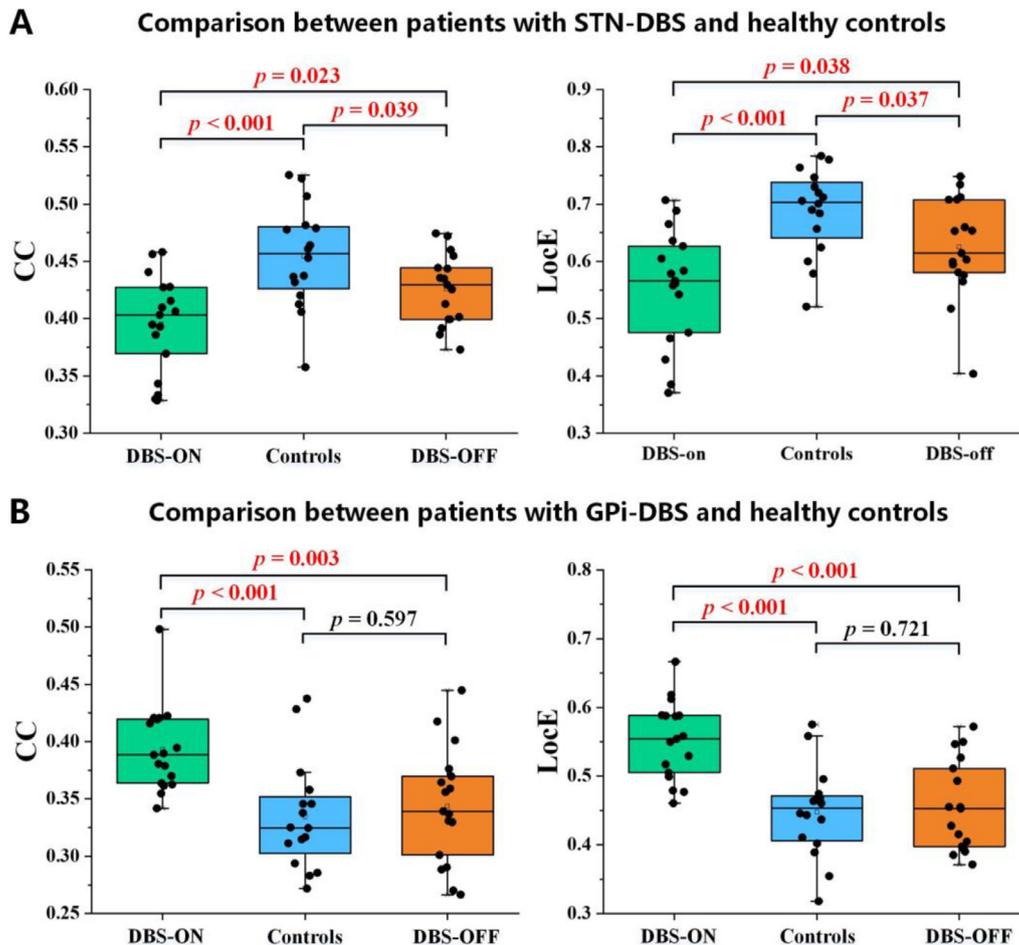

Fig. 4. Comparison of the characteristic non-motor network topology parameters between patients with Parkinson's disease and healthy controls. Comparing: (A) patients with Parkinson's disease treated with STN-DBS and healthy controls. (B) patients with Parkinson's disease treated with GPi-DBS and healthy controls. *P*-values marked in red indicate significant group differences ($p < 0.05$, FDR corrected). CC = clustering coefficient; Controls = healthy subjects; DBS-OFF = patients with Parkinson's disease with the deep brain stimulation (DBS) switched off; DBS-ON = patients with Parkinson's disease with the DBS switched on; FDR = false discovery rate; GPi = globus pallidus internus; LocE = local efficiency; STN = subthalamic nucleus.

CC and LocE of the patients' characteristic brain regions after DBS of the STN (Fig. 5A) were significantly lower than in the HC. The dynamic CC and LocE have significantly increased once the DBS was switched off but were still lower than in the HC. In contrast, for GPi DBS ON, the dynamic CC and LocE of the patients' characteristic brain regions after DBS of the GPi (Fig. 5B) were significantly higher than those of control subjects, and showed more clustered dynamic distribution; however, they decrease to the level of the HC when the DBS is OFF. This phenomenon corresponded to the above results, indicating that the DBS effects when

targeting the GPi and STN differed primarily in transforming the brain network properties. Furthermore, we noted different post-stimulation effects in the STN-DBS and GPi-DBS groups. Without the effect of GPi-DBS, the dynamic distributions of CC and LocE in the brain network of patients with Parkinson's disease in the GPi-DBS group have improved to be close to the level of the HC when in the DBS-OFF state. However, when the stimulator was switched off in patients in the STN-DBS group, CC and LocE distribution in their characteristic brain network remained significantly lower than in the HC.
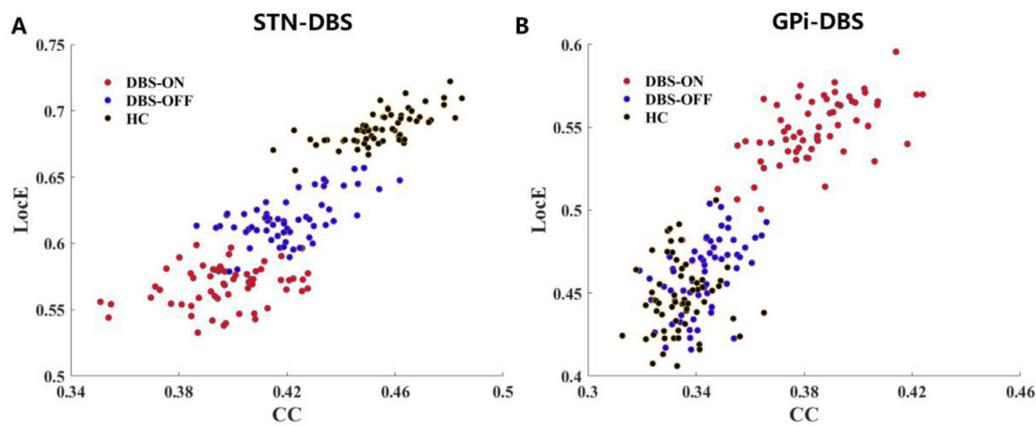
Fig. 5. Distribution of the characteristic non-motor network topology dynamic characteristics in the various groups (DBS-ON, DBS-OFF, healthy controls). (A) STN-DBS. (B) GPi-DBS. CC = clustering coefficient; DBS-OFF = patients with Parkinson's disease with the deep brain stimulation (DBS) switched off; DBS-ON = patients with Parkinson's disease with the DBS switched on; GPi = globus pallidus internus; HC = healthy controls; LocE = local efficiency; STN = subthalamic nucleus.

4. Discussion

In this study, we explored the topological changes of brain networks associated with deep brain stimulation in patients with Parkinson's disease, and compared reorganization patterns that emerge during stimulation of the GPi and the STN. Our results show that two parameters, namely, clustering coefficient and local efficiency, can be used to characterize topological reorganization occurring throughout the brain during active DBS. First, we show that DBS of either target leads to comparable improvements in motor function in individuals with Parkinson's Disease, and that these improvements are closely associated with the local efficiency of the anterior central gyrus and sensorimotor regions. Next, we show target-specific, divergent effects of DBS on the topological structure of non-motor brain regions. Specifically, STN-DBS significantly impairs information transmission ability (decreases local efficiency and leads to decentralization) of the inferior frontal gyrus angle, insula, temporal pole, superior occipital gyri, and posterior cingulate. Meanwhile, GPi-DBS improves information transmission in the cingulate gyrus, but decreases information transfer in the caudate and lenticular nucleus. Furthermore, we show that clustering coefficient and local efficiency of brain regions associate with cognitive function and mood remain lower than in healthy controls even after DBS is switched off, only in patients with STN-DBS. Meanwhile, the effects of GPi-DBS on the brain network appear to be transient, with the relevant indicators returning to normal levels once stimulation is switched off.

Using traditional small-world model and global network measures, we found that the brain functional networks of all participants, namely, individuals with Parkinson's disease during active stimulation to either target, stimulation to either target switched off, as well as healthy control subjects, exhibited small-worldness of the brain network, indicating that global organization of the brain network is preserved during deep brain stimulation. However, changes in the regional network during deep brain stimulation indicate significant topological reorganization of motor regions. Impaired local efficiency and decentralization are two known topological features of Parkinson's disease that appear early on in the disorder and worsen over time (Dubbelink et al., 2014). Our findings suggest that DBS works by increasing local efficiency of motor areas in both STN-DBS and GPi-DBS, and that these changes are clinically significant (as shown in Table 2 and Fig. 1). This finding expands upon other studies that report comparable results after DBS for either target, and suggest that topological reorganization of the motor cortex may be a useful measure of improved motor function with DBS in patients with Parkinson's disease, and a potential novel reference for optimizing the physiological characteristics of DBS.

Previous reports of cognitive and affective complications induced by DBS have been attributed to current spread into brain structures adjacent to the electrode, leading to inadvertent neural network activation (Kurtis et al., 2017; Obeso et al., 2008; Volkmann et al., 2010; Castrioto et al., 2014). Our findings indicate more extensive effects of STN-DBS than of GPi-DBS on non-motor areas, with a widespread loss in information transmission ability affecting the prefrontal cortex, insula, temporal pole, posterior cingulate, and occipital cortex (as shown in Fig. 3A, Fig 4A and Table 4). Other studies have found similar target-specific differences in both humans (Zhang et al., 2021) and animals (Min et al., 2012), with reports of changes in the cingulate cortex, insula, and occipital lobe during STN-DBS.

Interestingly, the present findings suggest that topological changes induced by active STN-DBS and GPi-DBS in non-motor regions associated with cognition and emotion are inverse (STN-DBS and GPi-DBS decrease and increase CC and LocE in non-motor regions, respectively), and may differ in terms of permanence (as shown in Fig 4B, Fig. 5 and Table 4). Of the two targets, STN-DBS is more commonly reported to induce adverse non-motor effects, including induce depression (Bejjani et al., 1999; Doshi et al., 2002; Schadt et al., 2006) and cognitive decline (Claeys et al., 2013; Mahdavi et al., 2014; Contarino et al., 2007). It is possible that our findings of increased decentralization and loss of local efficiency in limbic, paralimbic and association areas with STN-DBS could be related to cognitive and mood changes induced by stimulation of this target. In line with this, decentralization and decreased local efficiency of patients with depression have been reported for the whole brain network compared with healthy controls (Vincent et al. (Chen et al., 2017)), as well as specific regions, including posterior cingulate gyrus, angular gyrus, and inferior temporal cortex (Yicheng et al. (Long et al., 2020)). Meanwhile, decreased local efficiency and decentralization of regions in the fronto-parietal and cingulo-opercular networks have been observed in the early stage Parkinson's disease patients with cognitive impairment (Xiangbin et al. (Chen et al., 2020)). However, the relationship between topological reorganization and cognitive and affective changes associated with STN-DBS need to be further evaluated using behavioral tests.

Our results show a shift in centralization and local efficiency away from healthy controls for both target groups. However, while the shift in the STN-DBS group shows a decrease in both parameters consistent with an exacerbation of reduced topological centralization and efficiency already present in the off state, the GPi-DBS ON-state shows an increasing trend in these parameters from levels that largely overlap with healthy controls in the OFF-state. Although we cannot draw solid conclusions without behavioral data, these findings seem to align with previous evidence that GPi-DBS is not only less likely to induce mood deteriora-

tion and cognitive impairment than STN-DBS (Ramirez-Zamora and Ostrem, 2018; Wang et al., 2016), but may even improve PD patients' performance on certain cognitive tasks (Hansen et al., 2019). For example, Carbon et al. reported that in the cases of GPi-DBS, the improvement of patients' learning abilities is reflected in the increased brain network activities during the learning task (Carbon et al., 2003). Indeed, network activity increased with stimulation in GPi-DBS patients, suggesting enhanced functioning of higher order cognitive cortico-striato-pallidal-thalamocortical loops and related pathways (Carbon et al., 2003). We speculate that the shift in centralization and local efficiency of non-motor brain regions with GPi-DBS away from the level of healthy controls could be related to such beneficial effects on mood and cognition. However, whether this effect of GPi-DBS reflects the improvement of cognitive function, attention enhancement and other non-motor functional effects needs to be teased apart in further investigation.

Another key finding of the present study is that the effect of STN-DBS on non-motor topological features seem to persist after DBS is switched off, while the non-motor effects of GPi-DBS were not present in the OFF-state. The persistence of such topological changes in STN-DBS may reflect the response of brain functional networks to depression or cognitive deterioration in patients with long-term STN-DBS. While the temporary existence of such topological induced by GPi-DBS reflects that GPi-DBS does not cause substantial brain network topological changes related to depression or cognitive deterioration. However, due to the lack of baseline data before implantation and STN-DBS, follow-up studies would be required to verify this effect.

Dopamine D2 receptors are found in the striatum and are particularly concentrated in the outer segment of the globus pallidus. (Missale et al., 1998) It has been shown that a decrease in local efficiency of the striatum can be induced by blocking dopamine D2 receptors. (Achard and Bullmore, 2007) Meanwhile, it has also been shown that administration of levodopa (a drug known to increase dopamine levels) leads to a significant increase in local efficiency of the subcortical network in patients with Parkinson's disease (Berman et al., 2016), a network that includes basal ganglia structures with densely concentrated dopamine receptors. In the present study, we observed a significant reduction in local efficiency of the caudate nucleus and globus pallidus in the striatum during active GPi-DBS (as shown in Fig. 3B, Fig 4B and Table 4). This would be consistent with inhibited dopamine transmission with GPi-DBS, and also fits in well with clinical findings demonstrating that patients with GPi-DBS require higher doses of dopamine-enhancing drugs (Weaver et al., 2012; Moro et al., 2010; Odekerken et al., 2016).

The findings of this study should be considered in the context of its limitations. First, this work did not assess whether sex differences with STN or GPi target. The effects of DBS on the subjective pain perception of Parkinson's disease patients are known to be sex-specific, but it is not clear whether there are gender differences in other non-motor symptoms such as mood deterioration and cognitive decline. (Khazen et al., 2021) Second, PD patients recruited in this study were not randomized for target region. However, participants were recruited based on their earlier participation in one of two clinical trials conducted by our team. Each of these clinical trials investigated DBS intervention targeting one of the two brain regions compared in the present study. Importantly, recruitment criteria were identical in these trials. Moreover, the PD patients in two groups did not differ in the preoperative clinical manifestations, such as age, disease duration, levodopa response before DBS surgery, etc. Nevertheless, future investigation using randomized patient groups would be valuable. Finally, Parkinson's Disease is a heterogeneous disorder, and different disease characteristics may be associated with different neural responses to DBS. The neuroregulatory effects of DBS on different symptom dimensions of Parkinson's disease was not addressed in this study.

This is the first analysis of the neuromodulation effect of DBS on the resting state of brain network topology in patients with Parkinson's disease. We have found that subthalamic and pallidus stimulation induced topological reconfiguration in different non-motor functional brain regions, while their ability to improve motor function is similar. These results reveal the brain network topology characteristics underlying the clinical manifestations of STN-DBS and GPi-DBS, providing new insights into the neural response of Parkinson's disease to subthalamic and pallidus stimulation.

Credit authorship contribution statement

Chunguang Chu: Conceptualization, Methodology, Software, Formal analysis, Visualization, Writing – original draft, Writing – review & editing. **Naying He:** Conceptualization, Investigation, Resources, Visualization. **Kristina Zeljic:** Conceptualization, Visualization, Writing – original draft, Writing – review & editing. **Zhen Zhang:** Supervision, Project administration. **Jiang Wang:** Supervision, Project administration. **Jun Li:** Formal analysis, Visualization, Writing – review & editing. **Yu Liu:** Investigation. **Youmin Zhang:** Investigation. **Bomin Sun:** Supervision, Project administration. **Dianyou Li:** Supervision, Project administration. **Fuhua Yan:** Supervision, Project administration. **Chencheng Zhang:** Conceptualization, Resources, Writing – review & editing, Supervision, Project administration, Funding acquisition. **Chen Liu:** Conceptualization, Writing – review & editing, Project administration, Funding acquisition.

Ethics statement

The ethics committee of the Shanghai Ruijin Hospital approved all the study procedures (approval number: 2018017). All patients provided written informed consent following the Declaration of Helsinki.

Data availability statement

The fMRI data that support the findings of this study are available on request from the corresponding author. The data are not publicly available as they contain information that could compromise the privacy of research participants.

Supplementary materials

Supplementary material associated with this article can be found, in the online version, at doi:10.1016/j.neuroimage.2022.119196.

References

Chaudhuri, K.R., Healy, D.G., Schapira, A.H.V., 2006. Non-motor symptoms of Parkinson's disease: diagnosis and management. Lancet Neurology 5 (3), 235–245.

Deuschl, G., Schade-Brittinger, C., Krack, P., et al., 2006. A randomized trial of deep-brain stimulation for Parkinson's disease. New England Journal of Medicine 355 (9), 896–908.

Boutet, A., Madhavan, R., Elias, G., Joel, S.E., Lozano, A.M., 2021. Predicting optimal deep brain stimulation parameters for Parkinson's disease using functional MRI and machine learning. Nat Commun 12 (1).

Lachenmayer, M.L., Murset, M., Antih, N., et al., 2021. Subthalamic and pallidal deep brain stimulation for Parkinson's disease-meta-analysis of outcomes. Npj Parkinsons Disease 7 (1).

Bloem, B.R., Okun, M.S., Klein, C., 2021. Parkinson's disease. Lancet 397 (10291), 2284–2303.

Lozano, A.M., Lipsman, N., Bergman, H., et al., 2019. Deep brain stimulation: current challenges and future directions. Nature Reviews Neurology 15 (3), 148–160.

Limousin, P., Foltynie, T., 2019. Long-term outcomes of deep brain stimulation in Parkinson disease. Nature Reviews Neurology.

Bove, F., Mulas, D., Cavallieri, F., et al., 2021. Long-term Outcomes (15 Years) After Subthalamic Nucleus Deep Brain Stimulation in Patients With Parkinson Disease. Neurology.

Zhang, C.C., Wang, L.B., Hu, W., et al., 2020. Combined unilateral subthalamic nucleus and contralateral globus pallidus interna deep brain stimulation for treatment of Parkinson disease: a Pilot Study of Symptom-Tailored Stimulation. Neurosurgery 87 (6), 1139–1147.

Picillo, M., Lozano, A.M., Kou, N., Munhoz, R.P., Fasano, A., 2016. Programming Deep Brain Stimulation for Parkinson's Disease: the Toronto Western Hospital Algorithms. Brain Stimulation. 9 (3), 425–437.

L, S., L, G., J, O.V., et al., 2021. Subthalamic and pallidal deep brain stimulation: are we modulating the same network? [published online August 28, 2021]. Brain.

Zhang, C.C., Lai, Y.J., Li, J., et al., 2021. Subthalamic and pallidal stimulations in patients with Parkinson's disease: common and dissociable connections. Ann. Neurol. 90 (4), 670–682.

Dubbelink, K., Hillebrand, A., Stoffers, D., et al., 2014. Disrupted brain network topology in Parkinson's disease: a longitudinal magnetoencephalography study. Brain 137, 197–207.

Bassett, D.S., Bullmore, E.T., 2006. Small-world brain networks. Neuroscientist 12 (6), 512–523.

Stam, C.J., van Straaten, E.C.W., 2012. The organization of physiological brain networks. Clinical Neurophysiology 123 (6), 1067–1087.

Watts, D.J., Strogatz, S.H., 1998. Collective dynamics of 'small-world' networks. Nature.

van den Heuvel, M.P., Sporns, O., 2019. A cross-disorder connectome landscape of brain dysconnectivity. Nature Reviews Neuroscience 20 (7), 435–446.

Skidmore, F., Korenkevych, D., Liu, Y., He, G., Bullmore, E.T., Pardalos, P.M., 2011. Connectivity brain networks based on wavelet correlation analysis in Parkinson fMRI data. Neurosci. Lett. 499 (1), 47–51.

Baggio, H.C., Sala-Llonch, R., Segura, B., et al., 2014. Functional Brain Networks and Cognitive Deficits in Parkinson's Disease. Hum Brain Mapp 35 (9), 4620–4634.

Lebedev, A.V., Westman, E., Simmons, A., et al., 2014. Large-scale resting state network correlates of cognitive impairment in Parkinson's disease and related dopaminergic deficits. Front Syst Neurosci 8, 45.

Gorges, M., Muller, H.P., Lule, D., et al., 2015. To rise and to fall: functional connectivity in cognitively normal and cognitively impaired patients with Parkinson's disease. Neurobiol. Aging 36 (4), 1727–1735.

Luo, C.Y., Guo, X.Y., Song, W., et al., 2015. Functional connectome assessed using graph theory in drug-naive Parkinson's disease. J. Neurol. 262 (6), 1557–1567.

Putcha, D., Ross, R.S., Cronin-Golomb, A., Janes, A.C., Stern, C.E., 2015. Altered intrinsic functional coupling between core neurocognitive networks in Parkinson's disease. Neuroimage-Clinical 7, 449–455.

Gottlich, M., Munte, T.F., Heldmann, M., Kasten, M., Hagenah, J., Kramer, U.M., 2013. Altered Resting State Brain Networks in Parkinson's Disease. PLoS ONE 8 (10).

Berman, B.D., Smucny, J., Wylie, K.P., et al., 2016. Levodopa modulates small-world architecture of functional brain networks in Parkinson's disease. Movement Disorders 31 (11), 1676–1684.

Bullmore, E., Sporns, O., 2012. The economy of brain network organization. Nature Reviews Neuroscience 13, 336–349.

Latora, V., Marchiori, M., 2001. Efficient behavior of small-world networks. Phys. Rev. Lett. 87 (19).

Tinaz, S., Lauro, P., Hallett, M., Horovitz, S.G., 2016. Deficits in task-set maintenance and execution networks in Parkinson's disease. Brain Struct Funct 221 (3), 1413–1425.

Antonini, A., Abbruzzese, G., Ferini-Strambi, L., et al., 2013. Validation of the italian version of the movement disorder society-unified Parkinson's disease rating scale. Neurological Sciences 34 (5), 683–687.

Yan, C.G., Wang, X.D., Zuo, X.N., Zang, Y.F., 2016. DPABI: data processing & analysis for (resting-state) brain imaging. Neuroinformatics 14 (3), 339–351.

Ashburner, J., Friston, K.J., 2011. Diffeomorphic registration using geodesic shooting and Gauss-Newton optimisation. Neuroimage 55 (3), 954–967.

Friston, K.J., Williams, S., Howard, R., Frackowiak, R.S., Turner, R., 1996. Movement-related effects in fMRI time-series. Magn Reson Med 35 (3), 346–355.

Bassett, D.S., neuroscience, Sporns O.Network, 2017. Nat. Neurosci. 20 (3), 353.

Jin, M., Wang, L., Wang, H., Han, X., Wang, Z., 2021. Altered resting-state functional networks in patients with hemodialysis: a graph-theoretical based study. Brain Imaging Behav 15 (2).

Tommasin, S., Giglio, L.D., Ruggieri, S., et al., 2020. Multi-scale resting state functional reorganization in response to multiple sclerosis damage. Neuroradiology 62 (6), 693–704.

Wang, J., Wang, X., Xia, M., Liao, X., Evans, A., Yong, H., 2015. GRETNA: a graph theoretical network analysis toolbox for imaging connectomics. Front Hum Neurosci 9 (386), 386.

Tzourio-Mazoyer, N., Landeau, B., Papathanassiou, D., et al., 2002. Automated anatomical labeling of activations in SPM using a macroscopic anatomical parcellation of the MNI MRI single-subject brain. Neuroimage 15 (1), 273–289.

Erhardt, E.B., Rachakonda, S., Bedrick, E.J., Allen, E.A., Adali, T., Calhoun, V.D., 2011. Comparison of multi-subject ICA methods for analysis of fMRI data. Hum Brain Mapp 32 (12), 2075–2095.

Liu, F., Wang, Y.F., Li, M.L., et al., 2017. Dynamic functional network connectivity in idiopathic generalized epilepsy with generalized tonic-clonic seizure. Hum Brain Mapp 38 (2), 957–973.

Lu, F.M., Liu, C.H., Lu, S.L., et al., 2017. Disrupted topology of frontostriatal circuits is linked to the severity of insomnia. Front Neurosci 11.

He, Y., Dagher, A., Chen, Z., et al., 2009. Impaired small-world efficiency in structural cortical networks in multiple sclerosis associated with white matter lesion load. Brain 132, 3366–3379.

Collantoni, E., Meneguzzo, P., Solmi, M., Tenconi, E., Manara, R., Favaro, A., 2019. Functional connectivity patterns and the role of 5-HTTLPR polymorphism on network architecture in female patients with anorexia nervosa. Front Neurosci 13.

Kurtis, M.M., Rajah, T., Delgado, L.F., Dafsari, H.S., 2017. The effect of deep brain stimulation on the non-motor symptoms of Parkinson's disease: a critical review of the current evidence. Npj Parkinsons Disease 2.

Obeso, J.A., Rodriguez-Oroz, M.C., Benitez-Temino, B., et al., 2008. Functional organization of the basal ganglia: therapeutic implications for Parkinson's disease. Movement Disorders 23, S548–S559.

Volkmann, J., Daniels, C., Witt, K., 2010. Neuropsychiatric effects of subthalamic neurostimulation in Parkinson disease. Nature Reviews Neurology 6 (9), 487–498.

Castrioto, A., Lhommee, E., Moro, E., Krack, P., 2014. Mood and behavioural effects of subthalamic stimulation in Parkinson's disease. Lancet Neurology 13 (3), 287–305.

Min, H.K., Hwang, S.C., Marsh, M.P., et al., 2012. Deep brain stimulation induces BOLD activation in motor and non-motor networks: an fMRI comparison study of STN and EN/GPi DBS in large animals. Neuroimage 63 (3), 1408–1420.

Bejjani, B.P., Damier, P., Agid, Y., 1999. Transient acute depression induced by high-frequency deep-brain stimulation - Reply. New England Journal of Medicine 341 (13), 1004 1004.

Doshi, P.K., Chhaya, N., Bhatt, M.H., 2002. Depression leading to attempted suicide after bilateral subthalamic nucleus stimulation for Parkinson's disease. Movement Disorders 17 (5), 1084–1085.

Schadt, C.R., Cox, K.L., Tramontana, M.G., et al., 2006. Depression and intelligence in patients with Parkinson's disease and deep-brain stimulation. J Natl Med Assoc 98 (7), 1121–1125.

Claeys, I., Santens, P., Van den Abbeele, D., Van Roost, D., Lemmens, G.M.D., 2013. A manic episode after bilateral subthalamic stimulation in a patient with advanced Parkinson's disease. Acta Neuropsychiatr 25 (6), 367–369.

Mahdavi, R., Malakouti, S., Shahidi, G., Parvaresh-Rizi, M., Asadi, M., 2014. EPA-0030 – The effects of bilateral subthalamic nucleus stimulation on cognitive and neuropsychiatric functions in parkinson's disease: a case-control study. European Psychiatry 29.

Contarino, M.F., Daniele, A., Sibilia, A.H., et al., 2007. Cognitive outcome 5 years after bilateral chronic stimulation of subthalamic nucleus in patients with Parkinson's disease. Journal of Neurology Neurosurgery and Psychiatry 78 (3), 248–252.

Chen, V.C.H., Shen, C.Y., Liang, S.H.Y., et al., 2017. Assessment of brain functional connectome alternations and correlation with depression and anxiety in major depressive disorders. PeerJ 5.

Long, Y.C., Cao, H.Y., Yan, C.G., et al., 2020. Altered resting-state dynamic functional brain networks in major depressive disorder: findings from the REST-meta-MDD consortium. Neuroimage-Clinical 26.

Chen, X.B., Liu, M.T., Wu, Z.B., Cheng, H., 2020. Topological abnormalities of functional brain network in early-stage Parkinson's disease patients with mild cognitive impairment. Front Neurosci 14.

Ramirez-Zamora, A., Ostrem, J.L., 2018. Globus pallidus interna or subthalamic nucleus deep brain stimulation for Parkinson disease a review. JAMA Neurol 75 (3), 367–372.

Wang, J.W., Zhang, Y.Q., Zhang, X.H., Wang, Y.P., Li, J.P., Li, Y.J., 2016. Cognitive and psychiatric effects of STN versus GPi deep brain stimulation in Parkinson's disease: a meta-analysis of randomized controlled trials. PLoS ONE 11 (6).

Hansen, A.L., Krell-Roesch, J., Kirlin, K.A., et al., 2019. Deep Brain Stimulation and Cognitive Outcomes Among Patients With Parkinson's Disease: a Historical Cohort Study. Journal of Neuropsychiatry and Clinical Neurosciences 31 (3), 196–200.

Carbon, M., Ghilardi, M.F., Feigin, A., et al., 2003. Learning networks in health and Parkinson's disease: reproducibility and treatment effects. Hum Brain Mapp 19 (3), 197–211.

Missale, C., Nash, S.R., Robinson, S.W., Jaber, M., Caron, M.G., 1998. Dopamine receptors: from structure to function. Physiol. Rev. 78 (1), 189–225.

Achard, S., Bullmore, E.T., 2007. Efficiency and cost of economical brain functional networks. PLoS Comput. Biol. 3 (2), 174–183.

Weaver, F.M., Follett, K.A., Stern, M., et al., 2012. Randomized trial of deep brain stimulation for Parkinson disease Thirty-six-month outcomes. Neurology 79 (1), 55–65.

Moro, E., Lozano, A.M., Pollak, P., et al., 2010. Long-term results of a multicenter study on subthalamic and pallidal stimulation in Parkinson's disease. Movement Disorders 25 (5), 578–586.

Odekerken, V.J.J., Boel, J.A., Schmand, B.A., et al., 2016. GPi vs STN deep brain stimulation for Parkinson disease: three-year follow-up. Neurology 86 (8), 755–761.

Khazen, O., DiMarzio, M., Platanitis, K., et al., 2021. Sex-specific effects of subthalamic nucleus stimulation on pain in Parkinson's disease. J. Neurosurg. 135 (2), 629–636.